15

Planar Antenna Technology for mm-Wave Automotive Radar, Sensing, and Communications

Joerg Schoebel and Pablo Herrero
Braunschweig University of Technology
Germany

1. Introduction

Planar antennas are common components in sensing applications due to their low cost, low profile and simple integration with systems. They can be used commonly at frequencies as high as 77 GHz and above, for example in automotive sensing. Also, new ultra-wideband communication systems operating around 60 GHz will heavily rely on planar antennas due to their unique properties. One special advantage of planar elements is that they can easily form array structures combining very simple elements, like microstrip patches. Also phased and conformal arrays can be built. Due to all these characteristics, planar antennas are very good candidates for building front ends for mm-wave applications in radar, sensing or communications.

For some applications, which are either established today or which will become commercial in a few years, general requirements can be given. In addition to automotive radar, this mainly applies to 60 GHz ultra-broadband wireless indoor communications. Microwave imaging at 94 GHz and above is still much under research, as well as other sensing applications in the millimeter-wave region above 100 GHz. Prominent frequency bands are in the 122 and 140 GHz range[1].

Typical antenna requirements are multi-beam or scanning capability, high gain up to 30..36 dBi and moderate to low sidelobes. In monopulse radar systems, the sidelobes may be included in the angle determination scheme, then the sidelobe level requirements are rather relaxed.

Loss is generally an important issue. Comparing a planar approach to a commercially available dielectric lens, the planar antenna exhibits significantly higher losses, especially if the beamforming device is included. The antenna efficiency of 77 GHz planar array columns is roughly 50%. These losses are caused by dielectric losses and conductor losses. To attain reliable predictions of the losses in full-wave simulations, care has to be taken in the

[1] The FCC frequency allocations contain an amateur/mobile band at 122.25-123 GHz and an ISM (industrial, scientific, medical) band at 122-123 GHz. The bands 136-141 GHz and 141-148.5 GHz are allocated (among others such as radio astronomy) for amateur plus radiolocation and mobile plus radiolocation services, respectively by FCC and ECC. Therefore, a lot of bandwidth is within technological reach.

Source: Radar Technology, Book edited by: Dr. Guy Kouemou,
ISBN 978-953-307-029-2, pp. 410, December 2009, INTECH, Croatia, downloaded from SCIYO.COM

modeling of the conductors. Even if the conductors mainly are copper, a typical surface finishing consists of 3 to 5 μm nickel and a few hundred nanometers of gold. Comparing these numbers with the skin depth, it is found that a significant part of the current flows in the nickel. A layered impedance model for the metallization therefore improves the loss prediction significantly.
On the other hand, fabrication aspects have to be taken into account. Nickel acts as a diffusion barrier between gold and copper. Although practically not much interdiffusion will occur at room temperature, the nickel layer may still prove necessary as soon as wirebonding or other mounting technologies at elevated temperature are employed.
Generally planar antennas are well suitable for mass fabrication with low-cost processing. The required minimum feature sizes are realizable with common circuit board processes and the reproducibility of an industrial circuit board process is sufficiently good to achieve consistent antenna characteristics from lot to lot. For a low cost approach the RF functions should be limited to a single layer, which may be complemented with additional layers of low-frequency material (e.g. FR-4) for mechanical stabilization and accommodation of power supply and baseband circuitry.

2. Planar antennas for automotive radar applications

Due to the large number of groups working on planar antennas for automotive radar and the multitude of respective publications, an extensive review of the literature is not provided here. However, some examples for planar antenna implementations will be given below, which illustrate specific and interesting particular solutions.
Requirements for a multitude of different automotive-radar-based comfort and safety functions are compiled in (Mende & Rohling, 2002). While for the long range ACC applications an angular range of ±4° to ±8° is usually sufficient, short or medium range applications have different requirements in distance and angular range. The angular range is covered with a number of mutually overlapping beams intersecting approximately at their 3 dB points.
Conventionally, the beams are generated for example with a dielectric lens, which is fed from different positions in the focal plane. If the feed elements are realized as patches, a pre-focusing may be necessary for optimum illumination of the lens. This can be achieved with dielectric rods placed on top of the patches (Kühnle et. al., 2003). Fig. 2-1 a) shows the

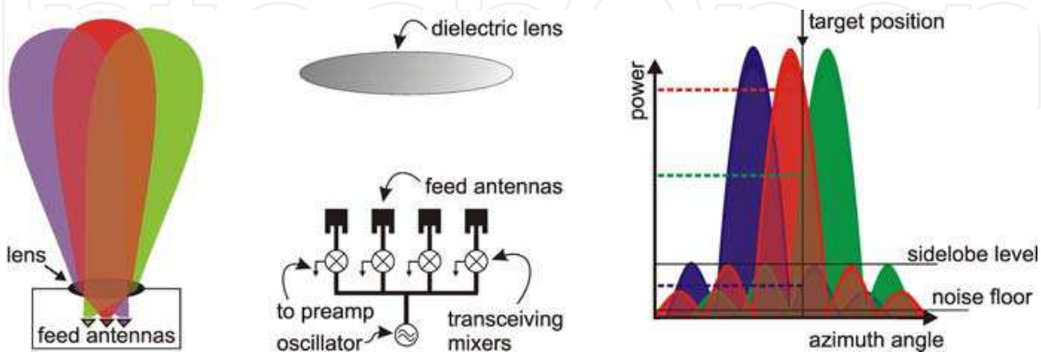

a) b) c)

Fig. 2-1. a) Beamforming in conventional lens-based radar systems; b) Block diagram of a lens-based automotive radar, c) Target angle determination with monopulse technique

concept of beam generation with a dielectric lens. A simple and low-cost circuit concept for an FMCW radar multi-beam front end is given in Fig. 2-1 b). All beams are illuminated simultaneously. The transmit signal also drives the transceiving mixers, which down convert the individual receive signals to baseband (Kühnle et. al., 2003).
The angular position of a radar target is determined by the amplitude ratio of the received signals in adjacent radar beams, typically referred to as monopulse technique, see Fig. 2-1 c). To achieve a reasonable angular accuracy, a number of 2 to 5 mutually overlapping beams is required to cover the azimuthal angular range of typical long or medium range applications. The beam width depends on the aperture size of the antenna, which is limited by practical reasons such as available mounting space at the bumper region.
Whereas the monopulse technique has shown excellent performance in automotive radar sensors for a long time, there are extensions and alternative algorithms, such as complex monopulse for multi-target situations (Schoebel, 2004b; Schoebel & Schneider, 2007) and high-resolution algorithms (Schneider et. al., 2002). Alternatively, a faster but less accurate determination of the target angular position can be realized using a larger number of beams and determining the target angle in a maximum search of the receive signals of the beams. In (Kawakubo et. al., 2004) a system providing pre-crash safety and ACC functions is described, which employs 41 digitally generated beams covering an angular range of ±10°.
A crucial point is the required radar range, which often exceeds 100 to 200 m. Concomitant to the narrow beam angles this also calls for a large antenna gain, which may exceed 30 dBi. As a result the size of a planar array may become quite large and special attention has to be paid to antenna and feed losses. Polarization is not very critical. Some systems use 45° polarization, so that radar signals from cars travelling in opposite directions and facing each other will be polarization decoupled to reduce interference. Alternatively, vertical polarization is less prone to multipath propagation between a car's bottom and the road surface (Schneider & Wenger, 1999), so that signal processing is facilitated by a complexity reduction of the radar scenario.
An early example of a Rotman lens employed for azimuthal beam forming in automotive radar is given in (Russell et. al., 1997). In elevation, series-fed columns are employed. Such planar antenna columns are elaborated in detail in (Freese et. al., 2000), where element widths are tapered to achieve a better sidelobe suppression (see examples in Fig. 3-2 a), b). 45° polarization is added to this concept in (Iizuka et. al., 2002) by employing inclined patches, which are connected to the feed line on a corner (see Fig. 3-2 c). A rather complex beam forming system based on several Rotman lenses was developed by (Metz et. al., 2001).

3. Design of patch elements, patch columns and arrays

3.1 Single patches

The design of single patch elements has been treated extensively in the literature (Balanis, 2005) and is not repeated here in detail. There are many methods for analyzing and designing patches, divided into empirical models, semi empirical models and full-wave analysis (Bhartia et. al., 1990). In this work, a rectangular patch is designed with the Transmission Line Model with the aid of a Matlab program to obtain a starting point for a parametric design with a full-wave simulator. With the substrate chosen (5 mil Ro3003), parameters of the simulation are patch width and length.
A single cell is here designed and simulated, in order to obtain the optimum parameters when connected in the array. The model consists of the rectangular patch with its initial

dimensions. The patch is connected from both sides with the high impedance microstrip lines. The impedance of this line is designed to be 100 Ohm, which will make feed arrangements easier. This impedance is equivalent for this substrate to a width of 85 μm, which can be processed with conventional "fine-feature" circuit board technology.
The patch model is tuned with the patch length to resonate at the desired operation frequency (e.g. around 140 GHz). The patch width is used for balancing the maxima of the E-field at the radiating edges of the patch (see Fig. 3-1 a). With the aid of the E-field diagrams and by deembedding the input port, the optimum line length is found for a 360° insertion phase between input and output of the cell. The respective input and output positions are located at the points where the field is minimum on the line (see arrows in Fig. 3-1 a). These calculations make the design of the final array arrangement and also the calculations of the number of elements very easy. A good design with very stable and processable dimensions is found. This model resonates at a frequency of 138 GHz (compare Fig. 3-1 b), so this model is chosen for designing the whole array.

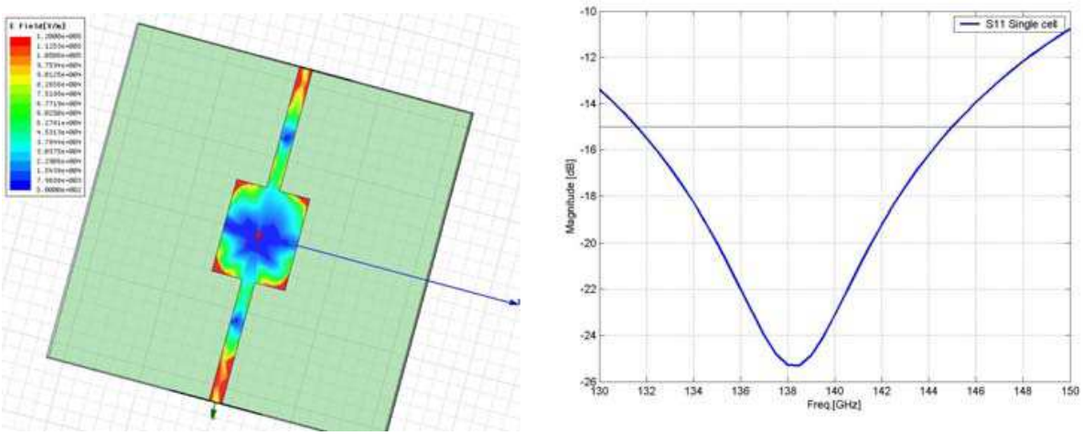

a) b)

Fig. 3-1. a) Single patch cell simulation for column design; b) Return loss of the patch cell

3.2 Patch array pattern modeling

Useful array patterns can be derived most straightforwardly by operating the patch in the ground (TM01) mode. Therefore, the radiation model needs to cover this mode only. (Carver & Mink, 1981) give analytical radiation patterns, which can easily be implemented in a numerical model. We implemented this model in a Matlab code, which allows to specify positions, excitation voltages, and phases of all individual patches in a planar array. Array patterns can easily be optimized or analyzed with this tool. Patch and feed losses are empirically taken into account in the excitation. Fig 3-2 e) gives antenna gain measurement and simulation of a single patch column of 20 elements in E and H planes. The correspondence is very good, only at very large angles some discrepancies can be seen, which are partly caused by the feed structure.
The designs presented in this work are all realized on 5 mil Ro3003 substrate. In the V and W bands this substrate is electrically sufficiently thin, so that surface waves play no significant role. Consequently, the pattern modeling may neglect surface waves and still reproduces the measured patterns very well (cf. Fig. 3-2 e). As patch antennas mainly excite

surface waves on their radiating edges in the E plane, the surface waves will travel along the series-fed column (see below) but their effect on the amplitude and phase of the excitation is negligible. The H plane azimuthal patterns are not much affected by surface waves, because their excitation from patch elements in this plane is low. Overall, the effect of surface waves is more pronounced at higher frequencies, in our case above 100 GHz. As the examples shown below are optimized in 3D or 2.5D simulations, partly for finite substrates, the effects of surface waves are implicitly taken into account.

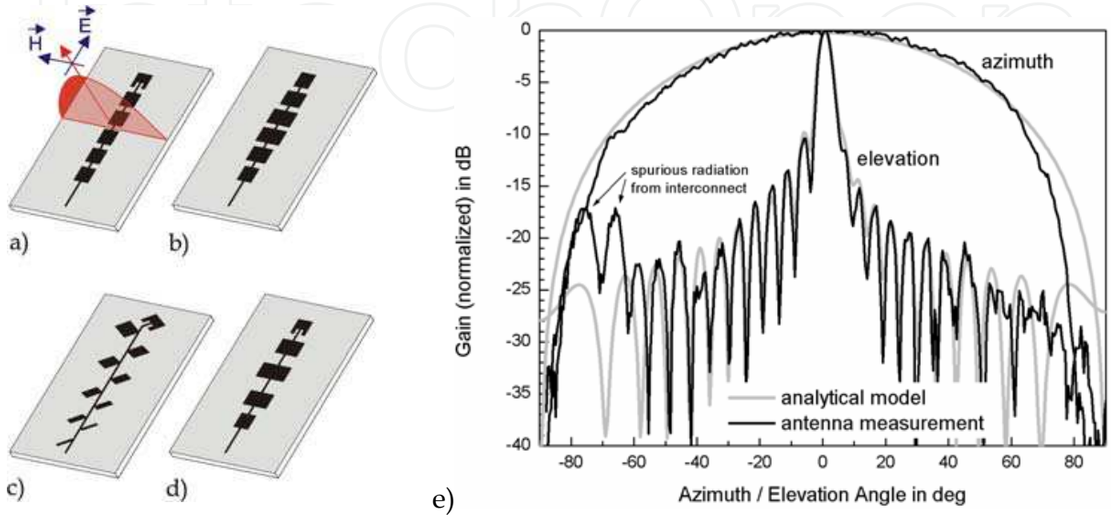

Fig. 3-2. a) Patch column with uniform series feed; b) Amplitude-tapered patch column; c) Amplitude-tapered inclined patch column; d) Phase and amplitude optimized column; e) Gain simulation and measurement of a 20-element patch column for 77 GHz

3.3 Series-fed columns

The mutual distance of the antenna columns in azimuth is restricted to not much more than half a free-space wavelength to suppress grating lobes, so the space for a feed network within each column is very limited. As the column consists of more than a few antenna elements, series feeding is the only possible approach and the series feed also has to provide the beam forming.

Once that the single patch cell is designed adjusting the complete column is easy. The most critical parameter affecting the matching of the whole array is the length of the high impedance line, because it ensures perfect impedance transformation at the edge of the patch. This length also contributes to the control of the phase distribution across the array and therefore influences the radiation profile.

Rectangular patches are used as antenna elements. They are directly coupled to the feed line at their edges and they are equidistantly placed on the column. As the input impedance of the feed point at the patch edge is rather large, the interconnecting lines are also designed for this impedance. The main beam should point in the broadside direction, so the interconnecting lines' lengths are adjusted for 360° phase shift between the input edges of consecutive patches (see cell design in section 3.1).

The feed point of the last element is shifted towards the inside of the element to provide a termination of the column (see Fig. 3-2 a). The inset length controls the global input reactance, so this parameter was used for improving the matching without much affecting

the center frequency. Finally, the length of the patch is slightly increased to decrease the resonant frequency.

3.4 Series-fed columns with uniform elements for 77 GHz

For the 77 GHz array, all elements on the column have the same size and emit approximately 10% of the respective input power except for the last element. Therefore, the power distribution on the column decreases exponentially except for the terminating element, which emits all the remaining power.

The phase distribution on the column (except the last element) is almost uniform with a small phase shift of approximately 3.3° between the elements. Far-field antenna pattern calculations for a 20-element column with the Matlab model described above are shown in Fig 3-2 e). As long as the phase distribution is uniform, the far-field pattern is symmetrical despite the unsymmetrical excitation amplitude pattern. The sidelobe level is between -9 to -11 dB for 10 to 20 elements. Due to the shifted feed point of the terminating element, a phase shift of this element with respect to the previous element of -50° occurs. The power emitted from the terminating element is a function of the number of elements in the column. This variation is sufficient to result in a visible squint of the main lobe and also in an unsymmetry of the pattern, as can be seen in Fig. 3-2 e).

This effect was studied experimentally. Fig. 3-3 a) shows antenna gain and squint angle as a function of the number of elements in the column. Due to the exponential power distribution and the element and inter-element losses, the gain tends to saturate for larger numbers of elements. The total loss of the column is around 2.5 dB for 20 elements. The squint is also reproduced satisfactorily taking into account an angular measurement uncertainty (antenna mounting and angular calibration) of approximately ±0.5° to ±1°. These results are confirmed in 3D electromagnetic simulations using HFSS.

3.5 Optimization of column patterns

An optimization of the elevation characteristics with respect to lowering the sidelobe level is beneficial for reducing the ground clutter, especially the near-range clutter from the road surface. To a lesser extent multi-path propagation due to reflections on the road surface will be mitigated. A straightforward solution is the implementation of a low-sidelobe excitation pattern on the series-fed column, as can be found for example in (Freese et. al., 2000). This can easily be achieved by variation of the patch width (cf. Fig. 3-2 b) and c). Due to the dependence of the available power of an element on the previous elements, antenna elements with rather large emission efficiencies are required. However, the maximum patch width is restricted by the excitation of the first transversal mode in the patch and also by a minimum distance between the columns of an array in order to suppress coupling between the columns.

For small patch widths, a reliable determination of the emission efficiency is difficult, because the radiated power is small and comparatively large measurement or numerical errors can easily occur in the development process. In general, the maximum achievable sidelobe suppression is a function of the maximum and minimum available patch widths.

An additional complication results from the matching of the patch elements, which requires a length adjustment as a function of patch width. Hence, for equidistant positions of the patches, phase errors are introduced, which deteriorate a low-sidelobe pattern. Adjusting the positions of the elements to ensure a uniform phase distribution will also affect the

antenna pattern as the spacing becomes non-uniform. Therefore, we propose an optimization procedure, which uses patch width and patch position as adjustable parameters to attain a low-sidelobe pattern with a series-fed antenna column. The excitation phase, which results from the position, is taken into account. Generally, this procedure will result in a non-uniform phase distribution and non-equidistant patch positions. It has been shown, that by controlling the phases of the elements of a linear array, an unsymmetrical pattern with low sidelobes on one side of the main beam can be achieved, even if the amplitude distribution is uniform (Trastoy & Ares, 1998). In an automotive application, only the sidelobes pointing to the road need to be reduced, therefore an unsymmetrical antenna pattern can be employed.

Fig. 3-3 b) shows antenna patterns calculated for Taylor 1-parameter and Chebyshev amplitude distributions for 8 elements implemented with a loss-free series feed and certain restrictions of maximum and minimum available patch widths. The excitation phase of all elements is assumed to be uniform. Due to the limitation of the range of available patch widths, the maximum sidelobe suppression is limited.

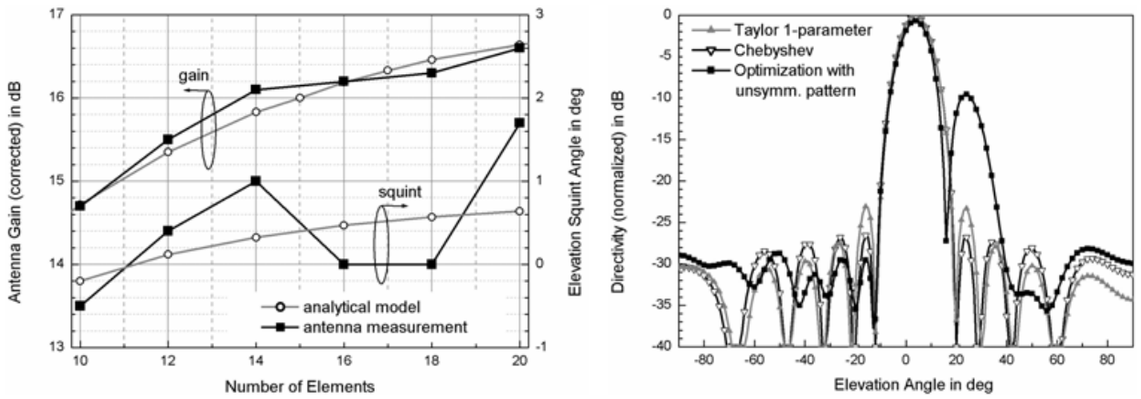

a) b)

Fig. 3-3. a) Antenna gain and elevation squint angle as a function of antenna elements in the column. The gain is corrected with respect to the loss of the feed line and interconnect;
b) Antenna patterns of series-fed columns restricted by the same maximum and minimum patch widths

Under the same conditions the patch widths and positions (and implicitly the excitation phases) are optimized for a low sidelobe level on one side of the main lobe. The optimization was implemented in Matlab using multidimensional nonlinear function minimization with Monte-Carlo and direct search algorithms. As a result, the first sidelobe level improves from -22.9 dB (Taylor one-parameter) or -26.4 dB (Chebyshev) to -28.8 dB. Correspondingly, the directivity reduces from 0 dB (Taylor, reference) or -0.2 dB (Chebyshev) to -0.7 dB.

It should be noted that to attain a low sidelobe level on a series feed, a similar optimization procedure has to be executed on a conventional amplitude distribution (such as Taylor or Chebyshev) in order to account for the changes in electrical and mechanical patch lengths, which result from the different patch emission efficiencies. Therefore, the improvement of the sidelobe level for the unsymmetrical pattern comes at virtually no extra effort in the design.

3.6 Patch array

To achieve a low sidelobe pattern in azimuth, the power divider feeding a corporate array has to generate a certain power distribution, here we choose a 20 dB Chebyshev pattern. In order to mitigate pattern distortions, which may be caused by reflections on the antenna input, the power divider is realized as a 3 stage Wilkinson setup employing uneven dividing ratios. As the size and parasitics of available thin-film resistors do not allow to mount them directly between the outputs, transformers are introduced between the resistor and the outputs of the dividers. This also allows to use other than the ideal resistor values. The complete divider is validated in an HFSS simulation including appropriate models of the resistors. Fig. 3-4 shows the HFSS model, the complete 8 column / 12 row array and a detail of the Wilkinson dividers with mounted resistors.

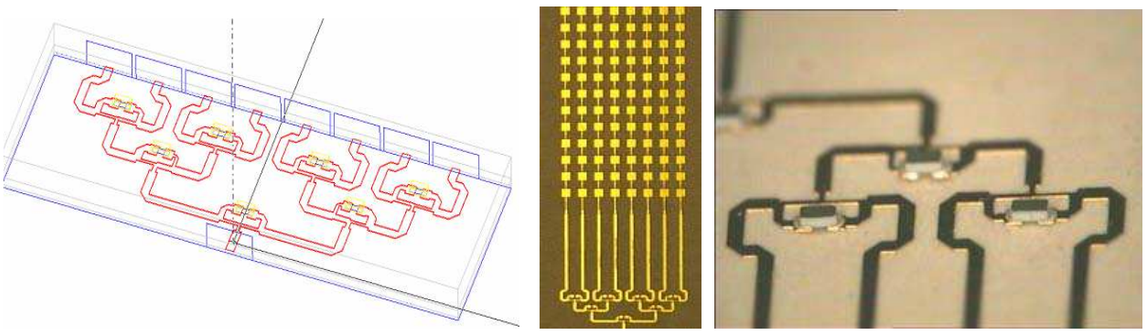

Fig. 3-4. HFSS model and photographs of circuit board layout and detail of Wilkinson divider with mounted resistors for an 8-output 20dB sidelobe level pattern

The dividers were analyzed on a wafer prober and excellent agreement of the power and phase distribution with the design was obtained. Results are given in Fig. 3-5. Amplitude tolerances amount to a maximum of ±7% and phase tolerances of ±6°, this is to be compared with probe placement tolerances of ±4°. The total loss is approximately 4.7 dB, where 1.5 dB are caused by radiation. The latter number was determined from HFSS simulations. The azimuthal pattern is given in Fig. 4-5 a).

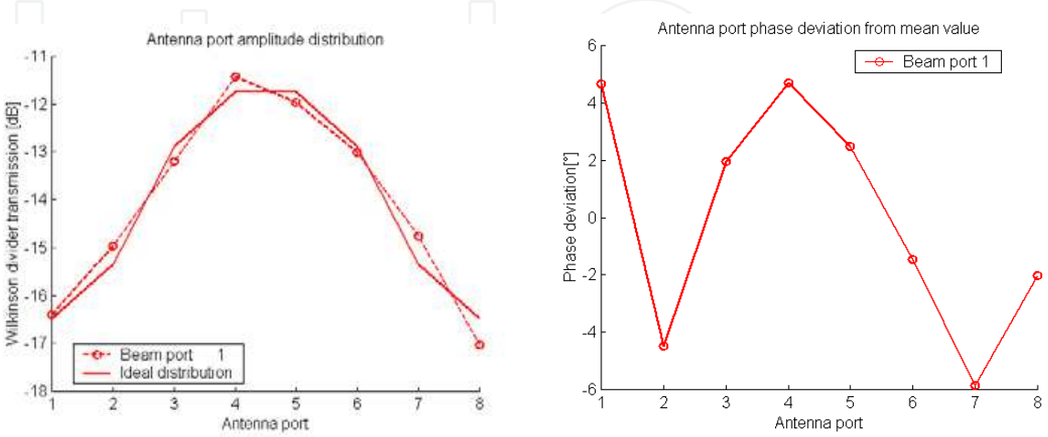

Fig. 3-5. Characterization results of 3-stage 8-output Wilkinson divider

4. Beam forming with planar Rotman lenses

In this chapter we present exemplary designs of a beam forming subsystem for automotive radar. These subsystems were originally intended to be used with a RF-MEMS based multi-throw switch, so that a single beam is active at a time (Schoebel et al., 2004 and 2005). But the same beam forming system can also be employed in an approach, in which all beams are active simultaneously (Hansen et al., 2006) similarly to the current automotive radar sensors as depicted in Fig. 2-1 b).

The planar Rotman lens consists of a parallel-plate waveguide with the beam ports on one side and antenna ports on the other side. The antenna ports are connected to the antenna elements via delay lines, which introduce an additional, individual phase shift. The lens has an ideal focus on its middle symmetry axis (shown red in Fig. 4-1 a) and two additional symmetrical ideal focal points. One is shown blue in Fig. 4-1 a) and the other one lies on a symmetrical position in the lower half. The focal lengths corresponding to the focal points can be different from each other.

Compared to an optical lens, the delay line network comprises the actual lens (position dependent phase shift), while the parallel plate waveguide corresponds to the free space region between the focal plane and the lens surface.

If additional beam ports are needed, focal spots are found on an approximately circular arc between and beyond the exact foci. In principle, the usable beam and antenna port contours extend to the point of their intersection (dashed in Fig. 4-1 a), but only the inner parts of these edge contours are used, as this improves the field distribution on the beam and antenna ports. The edges between the end points of the port contours are terminated (grey in Fig. 4-1 a), e.g. with microstrip ports, which are terminated at their ends. Rubber absorber glued on top of 1 to 2 cm of microstrip line is a practical termination for millimeter waves.

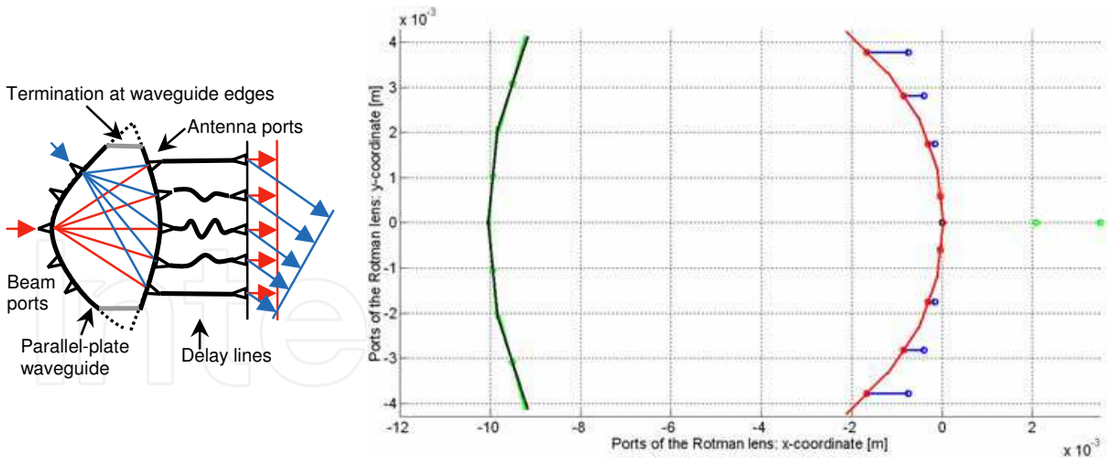

a) b)

Fig. 4-1. a) Operation principle of the Rotman lens, b) Analytical design of a Rotman lens

4.1 Design principle

The design of the Rotman lens is conducted using the classical analytical framework of (Rotman & Turner, 1963), which has been rewritten in terms of phase shift between the antenna elements. From the input parameters, such as desired phase shift, focal lengths and geometry and transmission line parameters the positions of the antenna ports and the

lengths of the delay lines are determined. In case that more beam ports than the 3 ideal foci are required, a numerical optimization of the positions of the additional beam ports is conducted. The result of the solution of the analytical design equations is shown in Fig. 4-1 b). The beam ports are located on the left and the antenna ports are on the right (circles). The delay lines are indicated by the horizontal lines at the antenna ports. The feed structures are microstrip tapers ("planar horn antennas") radiating into the parallel plate line. The front faces of the tapers are also shown in Fig. 4-1 b).

We use the total phase error (sum of absolute values of the phase deviation) versus position to determine the location of the non-ideal focusing points (beam ports) numerically. The same procedure is also employed at the ideal beam port foci and antenna ports[2]. Results are given in Fig. 4-2 a). Here, the results are restricted to two ports on one side of the lens; for the other two ports, the outcome is symmetrical. The dark spots give the location of the beam and antenna port foci. In our example, good phase accuracy is found for location tolerances of a few hundred micrometers. Generally, the light (yellow) regions indicate total phase deviations of a few degrees, which would generally be acceptable.

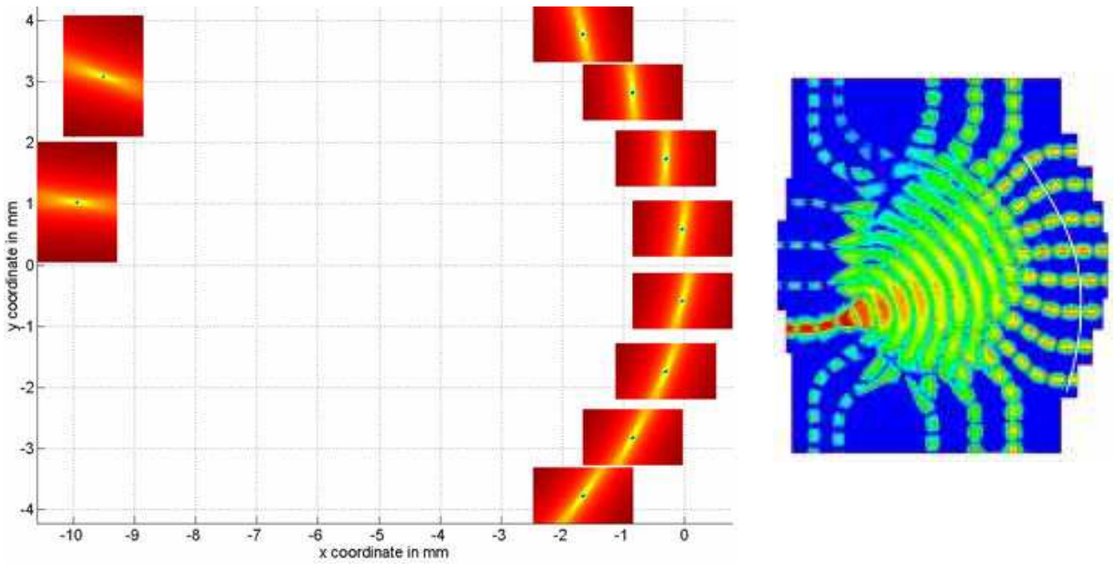

a) b)

Fig. 4-2. a) Phase errors versus port positions; b) 3D simulation of the electric field distribution in a Rotman lens. The white line indicates the phase shift of the antenna signals

It is interesting to note that the low phase error regions at the beam ports have the form of an elongated valley. As long as the beam port is on the bottom of this valley, low phase errors are obtained. From this observation, we can postulate a new design paradigm: the longitudinal orientation of the beam port feeding tapers should be along these valleys. In this case, uncertainties in the position of the phase centers of these tapers will have little influence on the lens performance, as the phase center of the taper will in any case be on its symmetry axis. Classically, the beam port faces are oriented tangentially on a circle around

[2] At the antenna ports the phase error is given by the deviation of electrical length between beam port and antenna port location. The latter is varied. In Fig. 4-2 a) the phase errors for all beam ports are added at each antenna port location.

the center of the antenna port contour (position (0,0) in Fig. 4-1b). The intersections of linear extrapolations of the valleys with the x axis are given in Fig 4-1 b) as circles to the right of the antenna port contour, also the beam port tapers' front faces are given for both cases[3] (black for the classical circular approach and green for orientation along the valleys).
Comparing the electrical lengths of the lens and delay line structure using the ideal focus points with the desired phase distributions on the antenna ports yields a very good agreement, as shown in Fig. 4-3 a).
The design of the feed tapers has to be conducted with some care. 3D or 2.5D simulations have to be employed to determine the phase centers of the tapers for different taper widths. The length of the tapers should be fixed to a value which ensures good matching, e.g. a few wavelengths. As the design is optimized empirically, the width of the tapers may change during the design process. As shown in Fig. 4-1 b) the width of the tapers is typically chosen so that negligible space between their edges remains.
Once the sizes of the feed tapers are know, the transmission in the parallel-plate waveguide can be modeled with a 2D radiation model as described in (Smith & Fong, 1983). The radiation characteristics of the tapers are calculated assuming a uniform E-field distribution at the front face. Taking into account the propagation path length and the overlap between beam and antenna port radiation patterns, the transmission properties of the lens and beam pointing losses are calculated. Results are given in Fig. 4-3 b).

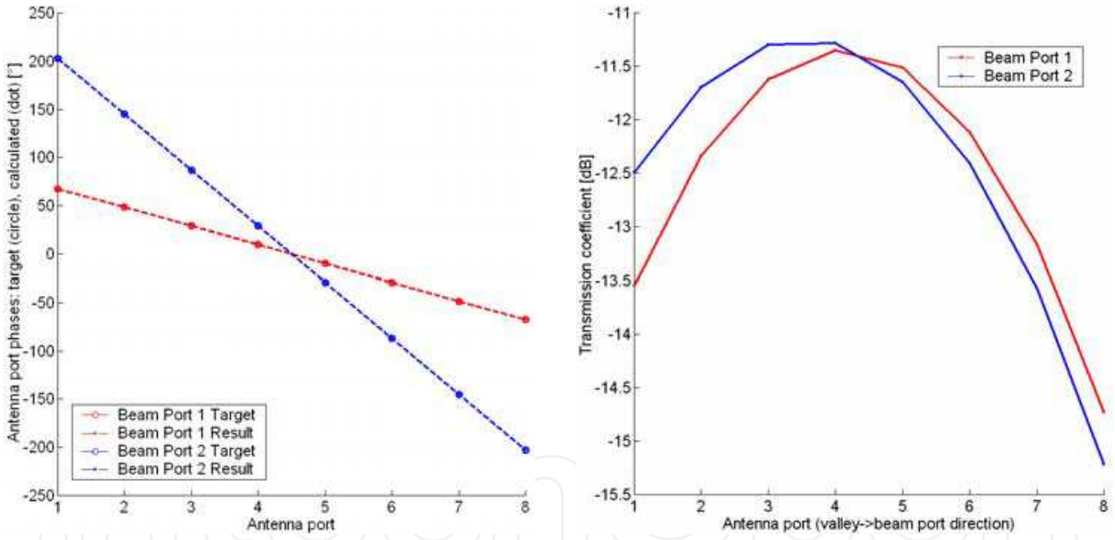

Fig 4-3. a) Antenna port phase distribution; b) Antenna port amplitude distribution

With these results, the lens is empirically optimized for optimum transmission. Typically we find that the focal lengths of on- and off-axis focal points should be equal. In addition, lateral extensions of beam and antenna port contours should also roughly be equal (compare Fig. 4-1). With the overall size of the lens the focusing of the port tapers can be controlled, as

[3] Here, the actual phase centers of the ports are not taken into account. In the final layout, the front faces of the tapers are somewhat shifted so that the phase centers of the tapers lie exactly on the focus points.

a larger feed will focus the radiation more strongly towards the middle of the opposite face of the parallel-plate waveguide. This may be used to control the sidelobe level.
Finally, the complete lens design can be validated in a 2.5D or 3D simulation, an example is given in Fig. 4-2 b).

4.2 Design examples

The design in Fig. 4-1 b) is conducted for 5 mil Ro3003 substrate ($\varepsilon = 3$) and 50 Ω delay lines ($\varepsilon_{eff} = 2.428$), focal lengths F=G=10 mm and 18° inclination between F and G. The figure is drawn to scale. The resulting beam pointing angles are ±6° and ±18° for an 8 element array in azimuth, which correspond to a prototypical short-to-medium range automotive radar application. The lens combined with 12-element antenna columns is depicted in Fig. 4-4 a) and the respective antenna pattern is presented in Fig. 4-5 a). This lens employs a conventional delay line network, which consists of a first, mostly linear section in order to change the lateral/azimuthal distance of the lines, so that their mutual distance is that of the final array ("Azimuthal distance control" in Fig. 4-4 b). Then, sinus-shaped sections are added, with which the specific delay is realized. The loss of the lens with delay line network amounts to approx. 4 dB.
Additional designs were conducted for long-range applications, for which a large antenna gain and beam angles of ±4° and ±8° are envisaged. Different focal lengths were tested, as can be seen in Fig. 4-4 a). If the size of the parallel-plate waveguide is made larger, the delay line network becomes shorter. We employ a novel routing scheme, which consists of a number of lines and circular arcs. This network is generally smaller than the conventional one and induces less radiation loss due to the larger radii of the arcs (compare Fig. 4-4 b).

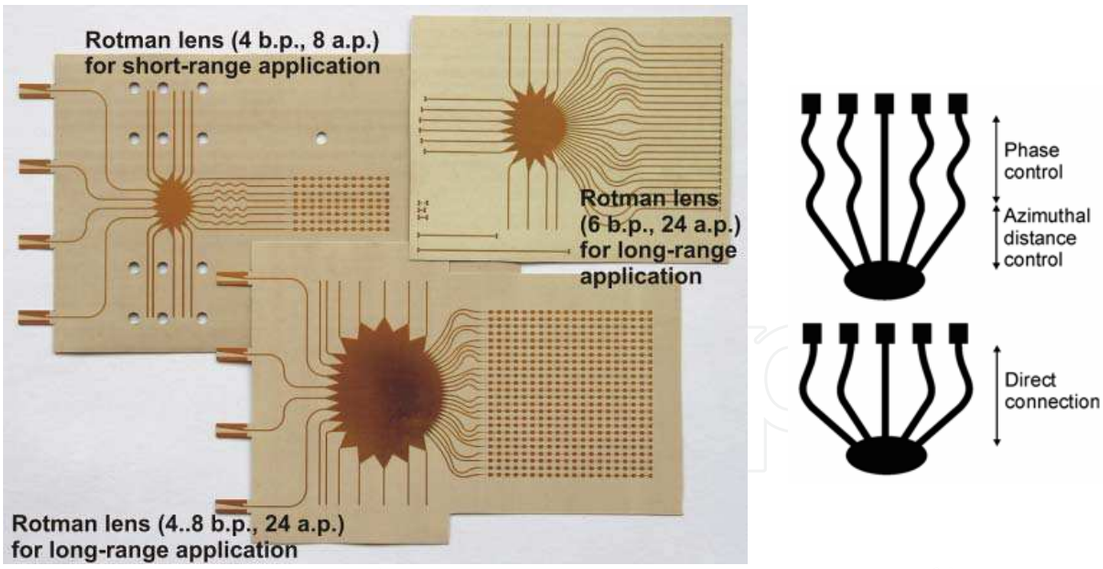

a) b)

Fig 4-4. a) Rotman lens examples for different automotive radar applications; b) Delay line network layout principles

Additionally, multiples of a guided wavelength are added towards the outer antenna ports, so that an additional amplitude taper comes in effect. This normally reduces the sidelobe level. Fig. 4-5 b) shows the antenna pattern of the largest lens in comparison to a commercial

dielectric-lens based radar sensor (Kühnle et. al., 2003). As can be seen, the pattern of the latter can be reproduced quite well by the inner four beams of the Rotman lens, but the overall gain of the Rotman-lens based antenna is smaller. The Rotman lens with delay line network induces losses of 6.5 dB.

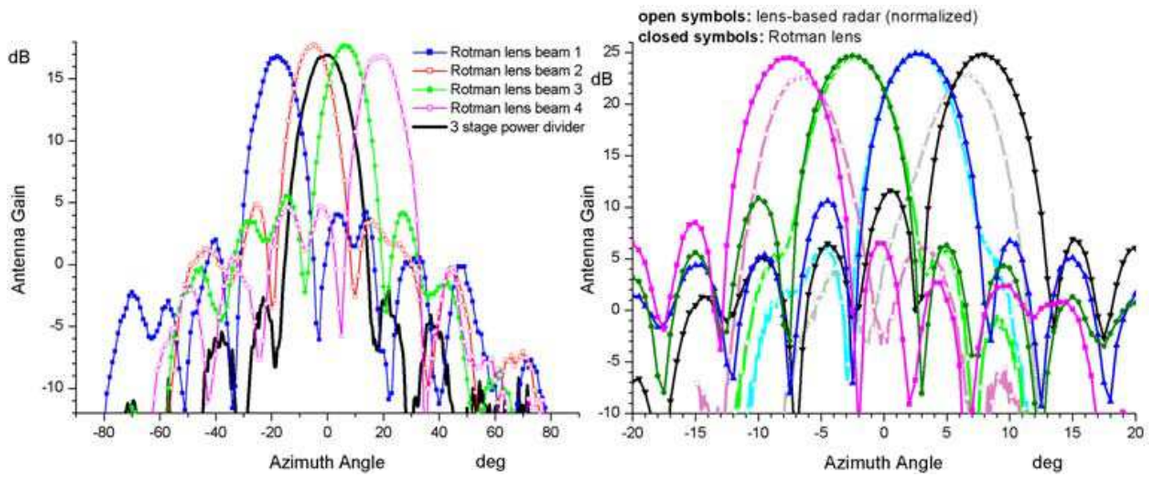

a) b)

Fig 4-5. a) Antenna patterns for Wilkinson divider and first Rotman lens; b) Antenna pattern for 8-beam-port Rotman lens (beams for the 4 inner beam ports are shown) compared to dielectric-lens based automotive radar system (gain maximum normalized to Rotman lens)

The design with 8 beam ports resulted from the empirical optimization of the lens performance. The desired 4 beam ports would occupy only a small part of the beam port contour, so additional ports were added. If the beam ports were increased in size, their radiation into the parallel-plate waveguide would be too much focused and would not illuminate the antenna ports at the edges sufficiently.

5. Patch antenna arrays for future automotive radar

5.1 Rationale

Even from the early beginning in automotive radar the key driver of all these investigations has been the idea of collision avoidance. Currently these systems are moving from autonomous cruise control and crash warning to real pre-crash reaction. Control systems of the vehicle (throttle, brakes) act when the radar system detects an unavoidable collision. The future concept of these systems is to create a virtual safety belt around the vehicle with multiple sensors, enhancing the current scenario towards the goal of autonomous driving. To achieve this goal, higher resolution radars and better accuracy is required.

A frequency of about 140 GHz is proposed here because radar antennas with better resolution and narrower beams than the actual 77 GHz sensors can be developed. Also, the very high frequency allows an easy integration, because the antenna size is very small. In addition, this band has been investigated as a serious candidate for future automotive radar systems (Schneider, 2007).

5.2 A case study for 140 GHz

The proposed antenna consists of a number of parallel patch columns, which are driven by a corporate feed network printed on one side of a grounded substrate as shown in Fig. 5.1 a) (Herrero et. al., 2008). Patches are connected by high impedance lines, while the main feeder is a 50 Ohm microstrip line. This feeding concept enables beam steering in an easy way and the area consumption is kept low. In this arrangement, the main lobe points to the broadside direction, which is usually required in an automotive radar antenna sensor. Moreover, as the main feeder is a corporate line, this direction is independent of the frequency. Sidelobe level in elevation should be low, as it determines the amount of clutter that the final system may have. The performance in this aspect was improved by using a tapered power distribution across the patch column, so more power is concentrated in the broadside direction. This is done by changing the width of the patch along the column.

For the single element, a patch antenna was chosen, because of its flexibility and easiness of design and fabrication. For designing the whole array, first a single cell was optimized for operation at a frequency of 140 GHz (see 3.1 above). The array calculator of HFSS was then used for finding the right number of cells for a 12 dBi gain array. The last patch was designed with an inset to allow an easy control of the whole antenna matching.

Results of matching show very good agreement between the simulated design and the measured one. The matching bandwidth (Fig. 5-1 b) is about 3 GHz, which is enough for a radar of this kind. Best matching is moved in frequency with respect to the original design due to inaccuracies of the lab-scale fabrication. Nevertheless, the fabrication process can be optimized because the behavior of the photolithography and etching process is very predictable. Also, a proper oversizing of layouts may be employed or dry etching techniques may be used. The radiation pattern measured also shows good agreement with the simulated one, showing a gain of about 11 dBi. A main lobe of about 20º width at -3 dB is observed, which makes the array suitable for short-to-medium range radar or other sensing applications.

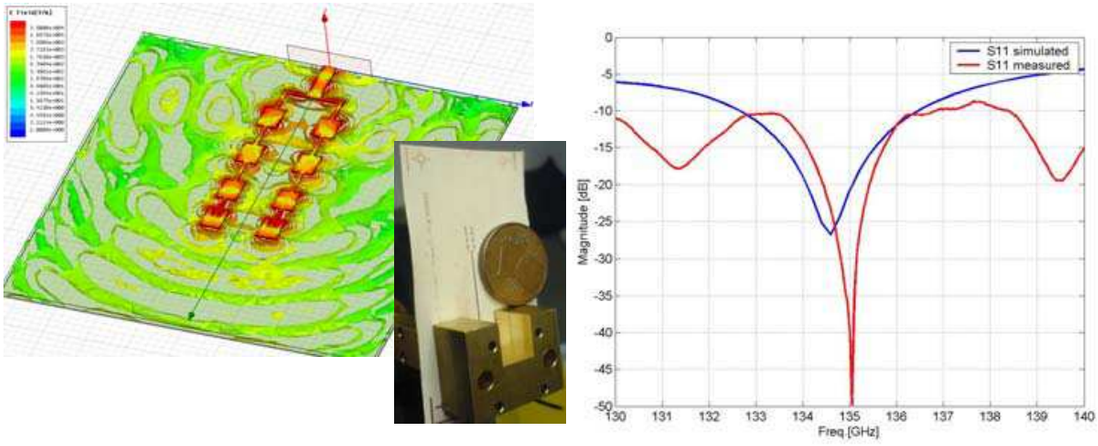

a) b)

Fig. 5-1. a) Prototypical 140 GHz array with E-field simulation and photograph compared to a 1-Eurocent coin; b) Return loss of the array

A setup for planar antenna measurement in the 110-170 GHz range was designed and realized in-house. It was used for all antenna measurements. The system is designed to measure return loss and radiation pattern in E and H planes in an accurate and repeatable way.
In consists of a vectorial network analyzer with external WR6 test heads, a rectangular waveguide-to-microstrip transition and some accessories, like a horn antenna and a rotary station controlled by a software programmed in python in conjunction with the network analyzer software.
The transition is proposed here as a low-cost solution for waveguide and microstrip interconnection and as a feed structure for planar antennas. Fig. 5-2 a) shows the concept of the proposed transition. It consists of a microstrip line printed on a dielectric substrate terminated with a radial stub. The ground plane of this microwave circuit has an H-shaped slot aligned with the waveguide aperture. Proper placement is achieved using alignment holes on the waveguide flange and a housing, which also contains a rectangular cavity designed to avoid power loss by back radiation. An H-shaped slot is used here to increase the bandwidth of the transition. It also contributes to improve the front-to-back radiation ratio. Moreover, the transition is easier to scale to other frequency ranges, contrary to a classical rectangular slot approach.

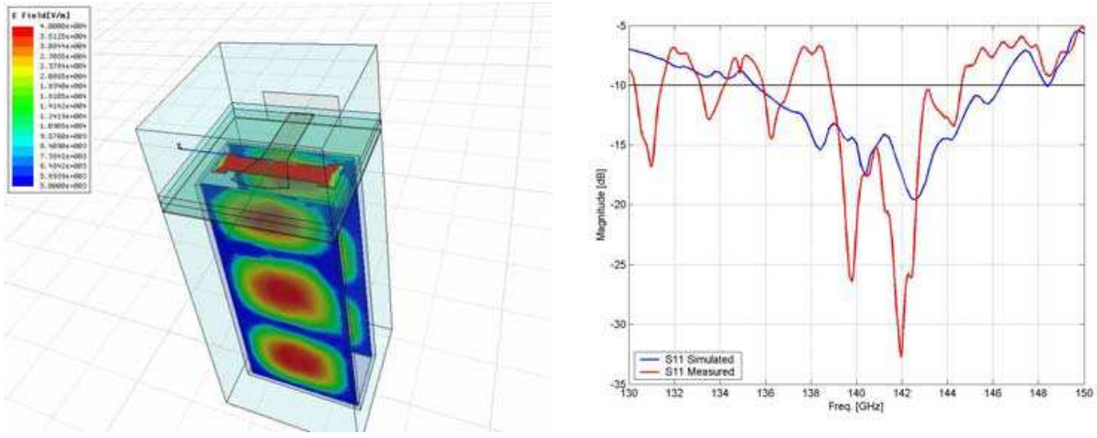

a) b)

Fig. 5-2. a) Concept of the waveguide to microstrip transition with E-field simulation;
b) Return loss of the waveguide port in the back-to-back double configuration

A value of 0.5 dB loss per interconnect can be obtained within the band of interest. Measured return loss yields a bandwidth around 10 GHz, typically enough for the requirements here. Matching also shows consistency between simulation and measurement. Performance of an exemplary transition centred at the frequency of 140 GHz is shown in Fig. 5-2 b). The fringes in the return loss are caused by standing waves in the characterized back to back configuration consisting of two transitions connected with a microstrip line.

6. Antennas for next generation applications in communications and sensing

In addition to the automotive radar, many other applications are expected to arise in the higher mm-wave range. In fact, an ISM (Industrial, Scientific and Medic) free to use band is allocated at the frequency of 122 GHz. This will partially solve the problem of the overcrowded spectrum in the low frequency ISM bands, like 2.45 GHz, where the current

most popular microwave systems work. The 122 GHz band will have at least 1 GHz of bandwidth, enough for various future sensing applications.
Probably the most appealing feature of going to such a high frequency would be the integration of systems. Sensors working at a frequency of 122 GHz can be even as tiny as the size of a coin, and therefore their integration possibilities increase substantially. Examples of these could be sensing devices for detecting gas particles, or microwave imaging systems. As an example, a very small sensor built in the safety belt, airbag cap, or dashboard of a regular car can improve the functionality of the airbag system by sensing distance and position of the persons in the front seats.

6.1 Patch antenna arrays

As demonstrated in the chapter above, planar antenna systems can be used at such high frequencies as 140 GHz. In this part we describe more patch arrays working at the frequency of 122 GHz for future sensing applications (Herrero et. al., 2009). Two arrays are presented, designed keeping in mind the typical requirements of a mm-wave radar sensor: low sidelobes for one antenna and scan capability for the other antenna.
Fig. 6-1 a) shows the concept of the proposed antennas. The first one shown is a serially fed patch array. The second one is a corporate fed patch array. The rectangular patch used as a single element in both arrays was chosen due to its simple design and manufacturing, and because is very flexible when building phased and conformal arrays.

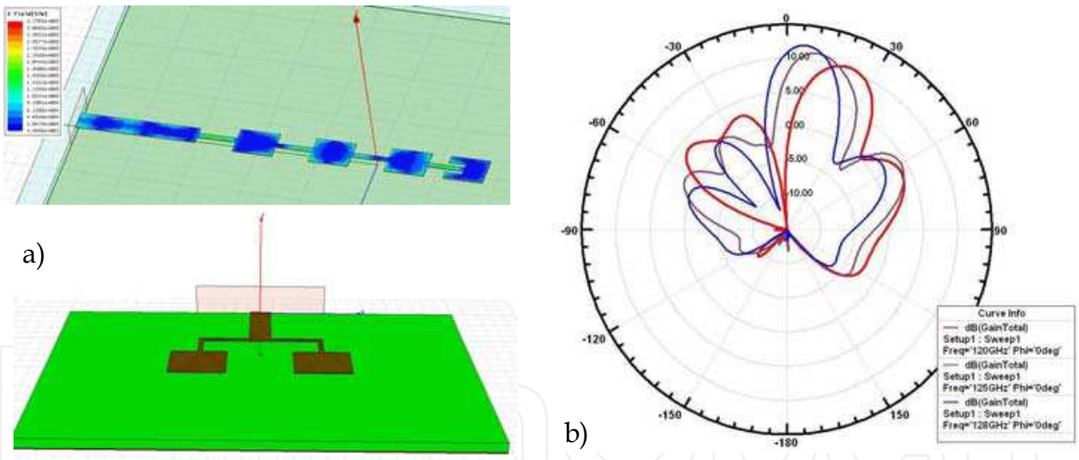

Fig. 6-1. a) Concepts of 122 GHz series and corporate feed arrays; b) Frequency-dependent E-plane antenna patterns of the series-fed array

The array column consists of a traveling wave transmission line, where fractions of power are coupled into the single elements. Last patch in the column is a matching element, avoiding the array to be a resonant array. This is done by introducing an inset in the patch, canceling the reactance at the microstrip main feed input. The whole configuration consumes very little area of substrate and it does not have impedance transformations, which keeps the loss of the feeding line low, which is important at such frequencies. This type of configuration allows beam steering in a simple way by changing the operating frequency of the array. The number of elements determine the scan range of the array

(Bhartia et. al., 1990) being 4 in this configuration. Simulated radiation patterns in Fig. 6-1 b) show the scan capability of the antenna.

The corporate line fed patch array consists in this case of one input and two outputs terminated by radiating patches. The power distribution chosen in this configuration is uniform. This is done by using a symmetrical structure, which also yields a uniform phase at the patch inputs. This makes the main beam independent of frequency, and points to the broadside direction. The width of the radiating elements was tuned so the matching to the high impedance line is optimum, improving the array's bandwidth.

For the measurements of the array column, we will focus on the elevation plane of the radiation pattern. The antenna has scan capability of the main lobe in this plane when changing the frequency of operation. Fig. 6-2 a) shows gain vs. angle and frequency in the E-plane. The scanning capability and range of the device can be clearly seen. Scan range is approx. between 25º and 5º with only four elements. Gain of the main lobe in this plane is about 6 dBi. Matching of the antenna is shown in Fig. 6-3 a) showing about 5 GHz bandwidth under -10 dB.

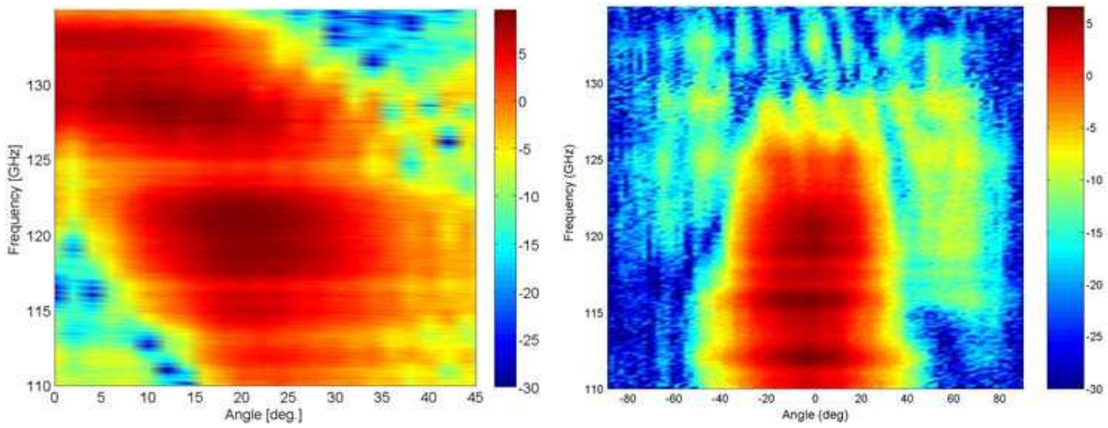

a) b)

Fig. 6-2. a) Frequency-dependent E-plane radiation pattern of the series-fed array;
b) Frequency-dependent H-plane radiation pattern of the corporate array

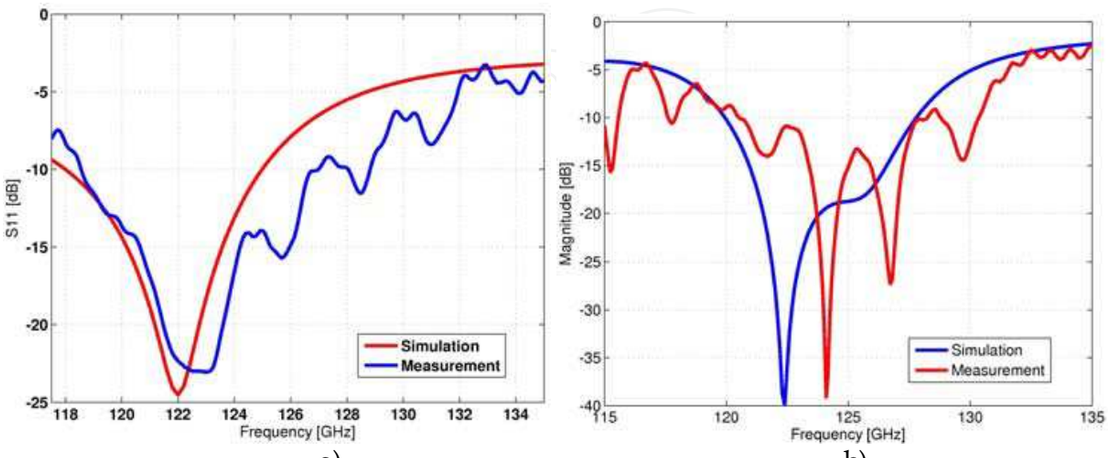

a) b)

Fig. 6-3. a) Return loss of the series-fed array; b) Return loss of the corporate array

For the corporate feed array configuration, return loss and both radiation patterns on E and H planes were measured. Matching of the antenna is depicted in Fig. 6-3 b) showing an excellent agreement between measurement and simulation. Bandwidth under -10 dB is about 7 GHz. A complete radiation profile including all the frequencies is shown in Fig. 6-2 b) for the in azimuth (H-) plane. It clearly shows two sidelobes more than -10 dB below the main beam. The radiation pattern is very stable for all frequencies. Subtracting losses of the transition and the microstrip line, which are known, the gain is found to be about 5 dBi.

6.2 Monopoles and dipoles

Another typical sensor antenna is the well known monopole. Planar monopoles yield a wide bandwidth, an omnidirectional radiation pattern, a simple low-profile structure and are easy to fabricate. Because of these reasons modern communication systems like UWB or WLAN use such antennas. In our case a metal strip of 100 µm width, extended above the ground plane and fed by a 50 Ohm microstrip line serves as radiating element (see Fig. 6-4 a). Different designs for 122 GHz were developed, fabricated and measured. Fig. 6-4 b) and Fig. 6-4 c) show the matching and the radiation patterns (H (yz) plane) of an exemplary antenna. The measured bandwidth accounts for 11 GHz between 121 and 132 GHz limited by the waveguide transition of the measurement setup. The simulation of the return loss in Fig. 6-4 b) yields a very large bandwidth of approx. ~30 GHz without the waveguide transition, so in the final application a similarly large bandwidth would be usable.

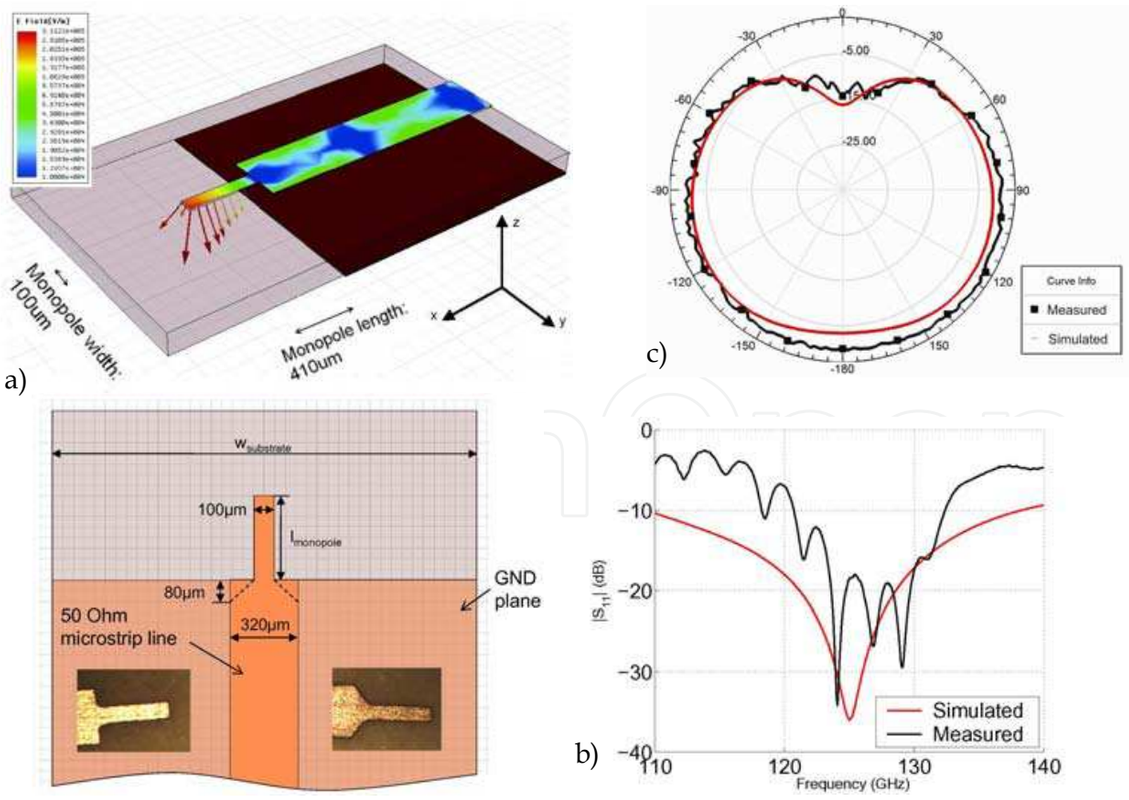

Fig. 6-4. a) Concept of the monopole with E-field simulation, dimensions and photographs; b) Return loss of the monopole; c) H (yz) plane radiation pattern

The microstrip dipole is a very good choice for integrating antennas and arrays in a future generation of high frequency applications. It is quite popular in WLAN systems because is intrinsically a quite broadband element, mandatory in bandwidth demanding applications. Also is a very compact and flexible structure when building arrays. In these, the level of cross coupling between elements is typically very low. Moreover, the structure is easily fabricated using conventional photolithography techniques.

Fig. 6-5 a) shows the concept of one of the proposed antennas. The double sided printed dipole consists of two arms formed by microstrip lines printed on different faces of a dielectric substrate and linear matching stubs (Tefiku & Grimes, 2000). The structure is fed by a 50 Ohm microstrip line. Its ground plane is truncated where the antenna element is connected to the line. The microstrip line is fed by a rectangular waveguide using a transition to microstrip line, allowing accurate and repeatable measurements.

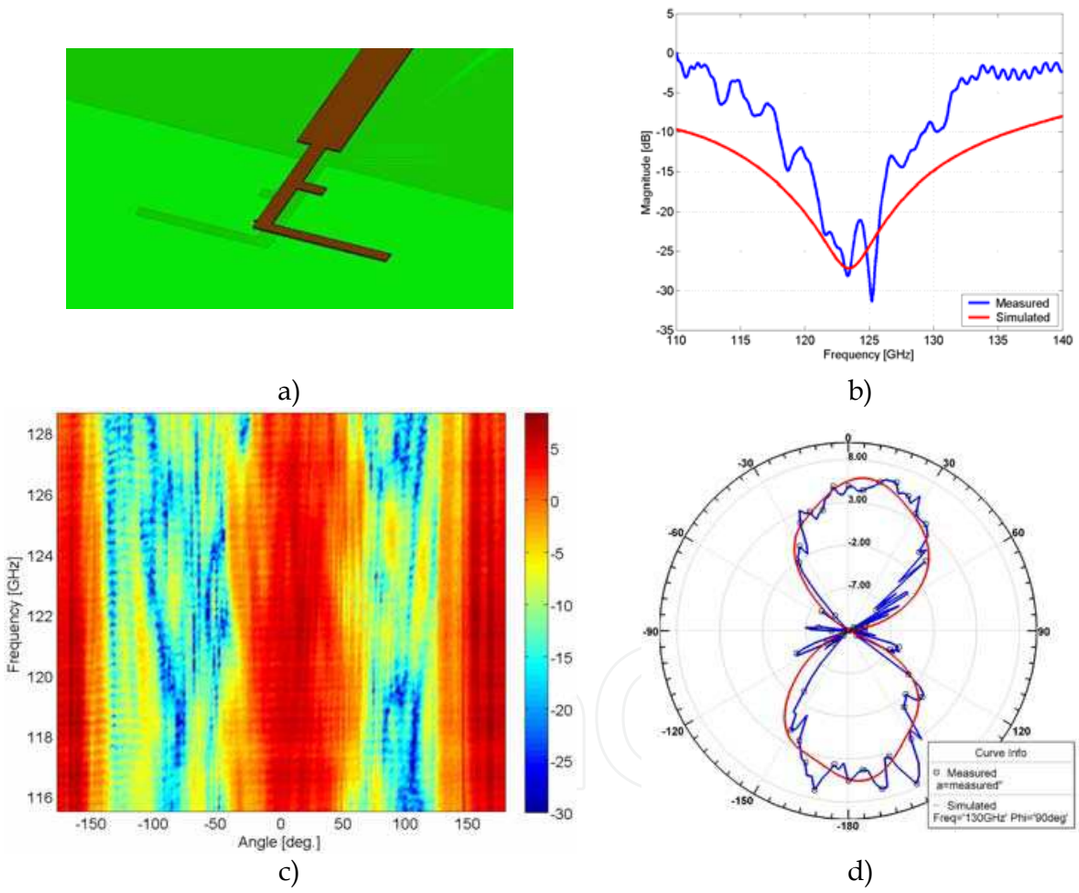

a) b)

c) d)

Fig. 6-5. a) Concept of the dipole; b) Return loss of the dipole; c) E plane radiation pattern versus frequency; d) E plane radiation pattern at 122 GHz

Key points in the design are the length of the dipole, which controls the main resonance. The length and width of the stub and the distance between the dipole and the stub are used to transform the "single ended" 50 Ohm microstrip line to the impedance of the dipole's balanced structure, thus acting as a balun. Dimensions of the whole structure are chosen keeping in mind also repeatable fabrication. The structure so designed is simple and does

not need a complicated balun to match the microstrip line. This balun usually consists of a tapered transition, which would be very complicated to implement at this frequency. The target frequency is around the 122 GHz ISM band. The bandwidth envisaged is at least 10 GHz for enabling future multimedia and communication applications (cf. matching in Fig. 6-5 b). The antenna is built on a commercial Rogers Ro3003 (12 μm metallization, 130 μm dielectric, ε = 3) substrate. Common photolithography tools and techniques are used in fabrication, yielding a very low-cost approach.
The radiation pattern observed is dipole like with two beams in the azimuth plane and a fan-like beam in the endfire directions (Fig. 6-5 d). The radiation characteristics are very uniform over the operation frequency range (Fig. 6-5 c). This characteristic, combined with the very integrable shape of the antenna makes the structure very suitable for future sensing systems using very wide bandwidths.

7. Conclusions

We have presented a selection of different planar antenna designs with different properties suitable for a multitude of applications in the higher mm-wave range.
Beamforming with power dividers or Rotman lenses was discussed in detail. We investigated the focusing properties of the Rotman lens and concluded with a new design concept for the positioning and orientation of the beam ports.
Smaller arrays and monopole and dipole elements were demonstrated in the 122 and 140 GHz ranges, which are interesting candidates for future applications in radar and sensing.
It was shown that a low-cost approach relying on commercial circuit board processes is feasible. The fabricated antennas generally exhibit properties very close to the design values, so detrimental effects such as fabrication inaccuracies and surface waves can be well under control, even for frequencies as high as 140 GHz.
The results shown in this work are generally also applicable to indoor ultra-wideband communications in the 60 GHz band. Here, antenna gains on the order of 15 dBi for transmitter and receiver are required to achieve a sufficiently high signal-to-noise ratio supporting data rates of several Gb/s under today's technological constraints (mainly transmitter power and receiver noise figure). Due to the high gain, the transmission is very directed and may be blocked, e.g. by moving people. This calls for beamsteering solutions such as the Rotman lens, which can be integrated in an essentially flat device setup. Ultimately, such a flat antenna front ends could be easily mounted on a laptop cover lid or in a PCMCIA card.

8. References

Balanis, C. (2005). *Antenna Theory: Analysis and Design,* 3rd ed., Wiley and Sons, 047166782X, Hoboken, New Jersey, USA

P. Bhartia, P.; Rao, K.V.S.; Tomar R.S. (1990). *Millimeter wave microstrip and printed circuit antennas*, Artech House, 0890063338, Boston, Massachusetts, USA

Carver, K.R.; Mink, J.W. (1981). Microstrip Antenna Technology, *IEEE Trans. Antennas Propagat.*, vol. AP-29, pp. 2-24

Freese, J.; Blöcher, H.-L.; Wenger, J.; Jakoby, R. (2000). Microstrip Patch Arrays for a Millimeter-Wave Near Range Radar Sensor, *Proc. German Radar Symposium GRS 2000*, pp. 149-153, Berlin, Germany, Oct. 2000

Hansen, T.; Schneider, M.; Schoebel, J.; Brueggemann, O. (2006). *Monostatic Planar Multibeam Radar Sensor*, WO2006/029926 A1.

Herrero, P.; Schoebel, J. (2008). Planar Antenna Array at D-Band Fed By Rectangular Waveguide for Future Automotive Radar Systems, *European Microwave Conference 2008*, Amsterdam, The Netherlands, October 2008.

Herrero, P.; Schoebel, J. (2009). Microstrip Patch Array Antenna Technology for 122 GHz Sensing Applications, *German Microwave Conference 2009*, Munich, Germany, March 2009.

Iizuka, H.; Sakakibara, K.; Watanabe, T.; Sato, K.; Nishikawa, K. (2002). Millimeter-Wave Microstrip Array Antenna with High Efficiency for Automotive Radar Systems, *R&D Review of Toyota CRDL*, Vol. 37, No. 2, pp. 7-12.

Kawakubo, A.; Tokoro, S.; Yamada, Y.; Kuroda, K.; Kawasaki, T. (2004). *Electronically Scanning Millimeter-Wave Radar for Forward Objects Detection*, SAE Technical Paper 2004-01-1122.

Kühnle, G.; Mayer, H.; Olbrich, H.; Steffens, W.; Swoboda, H.-C. (2003). Low-Cost Long-Range Radar for Future Driver Assistance Systems, *Auto Technology*, Issue 4/2003, pp. 2-5, ISSN 1616-8216

Mende, R.; Rohling, H. (2002). New Automotive Applications for Smart Radar Systems, *Proc. German Radar Symposium GRS 2002*, pp. 35-40, Bonn, Germany, Sept. 2002.

Metz, C.; Lissel, E.; Jacob, A.F. (2001). Planar multiresolutional antenna for automotive radar, *Proc. 31st European Microwave Conf.*, London, UK, October 2001

Rotman, W.; Turner, R.F. (1963). Wide-Angle Microwave Lens for Line Source Applications, *IEEE Trans. Antennas Propagat.*, vol. AP-11, pp. 623-632

Russell, M.E.; Crain, A.; Curran, A.; Campbell, R.A.; Drubin, C.A.; Miccioli, W.F. (1997). Millimeter-Wave Radar Sensor for Automotive Intelligent Cruise Control (ICC), *IEEE Trans. Microwave Theory Tech.*, Vol. 45, pp. 2444-2453

Schneider, M.; Groß, V.; Focke, T.; Hansen, T.; Brüggemann, O.; Schöberl, T.; Schoebel, J. (2002). Automotive Short Range Radar (SRR) Sensors at 24 GHz with Smart Antennas, *Proc. German Radar Symposium 2002*, pp. 175-179, Bonn, Germany, September 2002

Schneider, R.; Wenger, J. (1999). System aspects for future automotive radar, *IEEE MTT-S International Microwave Symposium 1999*, pp.293-296, Anaheim, California, USA, June 1999

Schneider, M. (2007). Advances in Microsystems Technology and RF Microelectronics for Highly Integrated 77 GHz Automotive Radar Sensors, *Workshop on Low-Cost, Integrated Automotive and Industrial Radar Sensors, International Microwave Symposium*, Honolulu, Hawaii, USA, June 2007

Schoebel, J.; Buck, T.; Reimann, M.; Ulm, M. (2004a). W-Band RF-MEMS Subsystems for Smart Antennas in Automotive Radar Sensors, *Proc. 34th European Microwave Conf.*, pp. 1305-1308, Amsterdam, The Netherlands, October 2004

Schoebel, J. (2004b). *Method of direction determination for multiple target situations for multi-lobe monopulse radar*, EP 1 500 952 B1.

Schoebel, J.; Buck, T.; Reimann, M.; Ulm, M.; Schneider, M.; Jourdain, A.; Carchon, G. and Tilmans, H. A. C. (2005). Design Considerations and Technology Assessment of RF-MEMS Systems in W-Band Smart Antenna Frontends for Automotive Radar Applications, *IEEE Trans. Microwave Theory Tech.*, Vol. 53, no. 6, pp. 1968-1975

Schoebel, J.; Schneider, M. (2007). Smart antennas for automotive radar front-ends: from beam steering to high-resolution algorithms, *Workshop on Smart Antennas, European Microwave Conference 2007*, Munich, Germany, October 2007.

Smith, M.S.; Fong, A.K.S. (1983). Amplitude Performance of Ruze and Rotman Lenses, *The Radio and Electronic Engineer*, vol. 53, No. 9, pp. 329-336

Tefiku, F. and Grimes, C. (2000). Design of broad band and dual band antennas comprised of series fed printed strip dipole pairs, *IEEE Trans. Antennas and Propagat.,* vol. 48, pp. 895–899

Trastoy, A.; Ares, F. (1998). Phase-only synthesis of continuous linear aperture distribution patterns with asymmetric side lobes, *Electron. Lett.*, vol. 34, pp. 1916-1917

Radar Technology

Edited by Guy Kouemou

ISBN 978-953-307-029-2
Hard cover, 410 pages
Publisher InTech
Published online 01, January, 2010
Published in print edition January, 2010

In this book “Radar Technology”, the chapters are divided into four main topic areas: Topic area 1: “Radar Systems” consists of chapters which treat whole radar systems, environment and target functional chain. Topic area 2: “Radar Applications” shows various applications of radar systems, including meteorological radars, ground penetrating radars and glaciology. Topic area 3: “Radar Functional Chain and Signal Processing” describes several aspects of the radar signal processing. From parameter extraction, target detection over tracking and classification technologies. Topic area 4: “Radar Subsystems and Components” consists of design technology of radar subsystem components like antenna design or waveform design.

How to reference

In order to correctly reference this scholarly work, feel free to copy and paste the following:

Joerg Schoebel and Pablo Herrero (2010). Planar Antenna Technology for mm-Wave Automotive Radar, Sensing, and Communications, Radar Technology, Guy Kouemou (Ed.), ISBN: 978-953-307-029-2, InTech, Available from: http://www.intechopen.com/books/radar-technology/planar-antenna-technology-for-mm-wave-automotive-radar-sensing-and-communications

INTECH
open science | open minds

InTech Europe
University Campus STeP Ri
Slavka Krautzeka 83/A
51000 Rijeka, Croatia
Phone: +385 (51) 770 447
Fax: +385 (51) 686 166
www.intechopen.com

InTech China
Unit 405, Office Block, Hotel Equatorial Shanghai
No.65, Yan An Road (West), Shanghai, 200040, China
中国上海市延安西路65号上海国际贵都大饭店办公楼405单元
Phone: +86-21-62489820
Fax: +86-21-62489821

IntechOpen